Vietnam Journal of Mechanics, Vol. 44, No. 4 (2022), pp. 431 – 444
DOI: https://doi.org/10.15625/0866-7136/17933

NONLINEAR BUCKLING ANALYSIS OF HIGHER-ORDER SHEAR DEFORMABLE FG-CNTRC PLATES STIFFENED BY OBLIQUE FG-CNTRC STIFFENERS

Tran Quang Minh[1,*], **Vu Minh Duc**[1], **Dang Thuy Dong**[2], **Vu Hoai Nam**[2]
[1]*Institute of Transport Technology, University of Transport Technology, Hanoi, Vietnam*
[2]*Faculty of Civil Engineering, University of Transport Technology, Hanoi, Vietnam*
[*]E-mail: minhtq@utt.edu.vn

Received: 05 December 2022 / Published online: 30 December 2022

Abstract. The nonlinear buckling analysis of functionally graded carbon nanotube-reinforced composite (FG-CNTRC) plates subjected to axial compression load is analytically examined in this paper. Assuming that the FG-CNTRC plates are stiffened by an oblique FG-CNTRC stiffener system. Reddy's higher-order shear deformation plate theory (HSDPT) with the geometrical nonlinearities of von Kármán is applied to establish the basic formulations. Moreover, the smeared stiffener technique is successfully improved for the higher-order shear deformable anisotropic oblique stiffener system by using a homogeneous model of the anisotropic beam. Galerkin's method is used to achieve the expressions of critical buckling loads and postbuckling load-deflection curves in explicit form. The numerical values display the influences of FG-CNTRC stiffeners, material, and geometrical properties on the nonlinear buckling response of plates.

Keywords: buckling and postbuckling, nonlinear, functionally graded carbon nanotube-reinforced composite, plate, higher-order shear deformation theory, oblique stiffener.

1. INTRODUCTION

Due to the superior thermal-mechanical characteristics, the functionally graded carbon nanotube-reinforced composites (FG-CNTRC) have special importance in complex industries. Therefore, the problems of nonlinear buckling of FG-CNTRC plates are worthy of interest because of their important role in engineering designs.

The mechanic buckling and postbuckling behavior of FG-CNTRC plates was studied by Shen and Zhu [1], Zhang et al. [2], and Zghal et al. [3] using different methods and different shear deformation theories. Shen and Zhang [4] and Mirzaei and Kiani [5] investigated the linear and nonlinear thermal buckling behavior of FG-CNTRC plates. The nonlinear vibration problems of FG-CNTRC plates were also mentioned by Shen and Wang [6], and Mirzaei and Kiani [7]. For the stiffened plates, the functionally graded

plates stiffened by orthogonal, and oblique stiffeners were analyzed in nonlinear buckling problems with the development of the improved smeared stiffener techniques for first- and higher-order shear deformation theories [8–10].

In this paper, the stiffener designs are proposed for FG-CNTRC plates stiffened by FG-CNTRC stiffeners. A new higher-order shear deformable anisotropic smeared stiffener technique is developed in this paper using a homogeneous model of the laminated beam where the stiffener design of FG-CNTRC structures is applied. The effects of FG-CNTRC stiffeners involved distribution laws of CNT, volume fraction, and stiffener types on the buckling behavior of the FG-CNTRC plate stiffened by FG-CNTRC stiffeners are analysed and discussed in numerical investigations.

2. GEOMETRICAL AND MATERIAL PROPERTIES AND SOLUTION PROBLEMS

Consider a stiffened FG-CNTRC plate under axial compression P_x made of isotropic polymer matrix and reinforced by single-walled carbon nanotubes (SWCNTs). As shown in Fig. 1, the coordinate system $Oxyz$ is chosen with the geometrical parameters of stiffeners include h_l is height, b_l is width, and d_l is the distance between the two adjacent stiffeners. The carbon nanotubes (CNTs) are designed in x-directions of the plates. θ is the angle between the stiffeners and the x-axis.

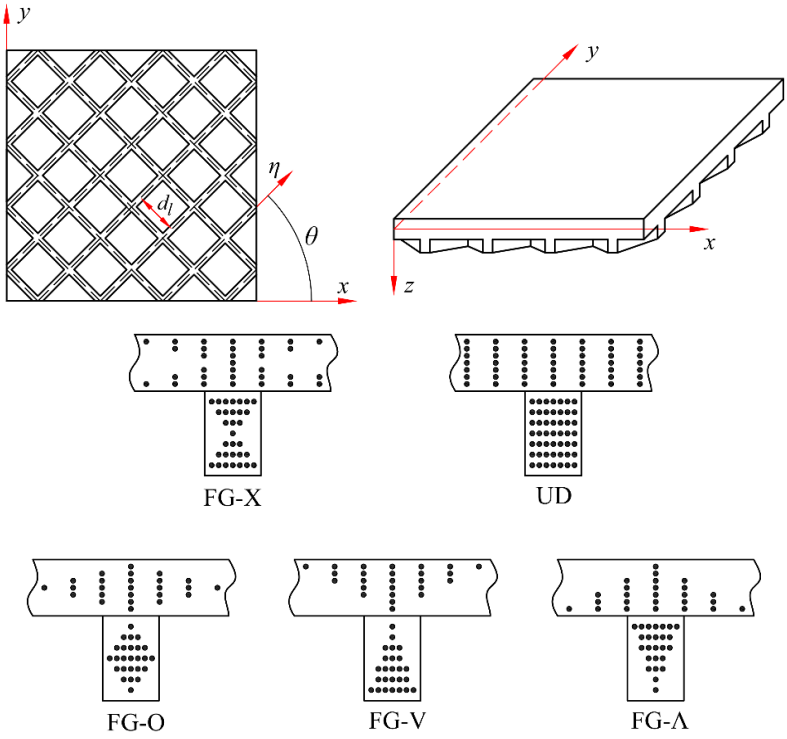

Fig. 1. FG-CNTRC plates with FG-CNTRC oblique stiffeners and CNT distribution laws in plate and stiffeners

Five linear distributions of CNTs are considered for plate-stiffener structure (see Fig. 1), according to the following formulations, as

- FG-X type:

$$+ \text{For plate} \qquad V_{CNT} = 4V^*_{CNT}\frac{|z|}{h} \qquad \text{with } -h/2 \le z \le h/2, \tag{1}$$

$$+ \text{For stiffeners } V_{CNT} = 2V^*_{CNT}\left|\frac{-2z+h}{h_l}+1\right| \text{ with } \quad h/2 \le z \le h/2+h_l. \tag{2}$$

- FG-O type:

$$+ \text{For plate} \qquad V_{CNT} = 2V^*_{CNT}\left(1-\frac{2\,|z|}{h}\right) \qquad \text{with } -h/2 \le z \le h/2, \tag{3}$$

$$+ \text{For stiffeners } V_{CNT} = V^*_{CNT}\left(1-\left|\frac{2z-h}{h_l}-1\right|\right) \text{ with } \quad h/2 \le z \le h/2+h_l. \tag{4}$$

- UD type:

$$+ \text{For plate} \qquad V_{CNT} = V^*_{CNT} \text{ with } -h/2 \le z \le h/2, \tag{5}$$

$$+ \text{For stiffeners } V_{CNT} = V^*_{CNT} \text{ with } \quad h/2 \le z \le h/2+h_l. \tag{6}$$

- FG-V type:

$$+ \text{For plate} \qquad V_{CNT} = V^*_{CNT}\left(-\frac{2z}{h}+1\right) \text{ with } -h/2 \le z \le h/2, \tag{7}$$

$$+ \text{For stiffeners } V_{CNT} = V^*_{CNT}\left(\frac{2z-h}{h_l}\right) \quad \text{with } \quad h/2 \le z \le h/2+h_l. \tag{8}$$

- FG-Λ type:

$$+ \text{For plate} \qquad V_{CNT} = V^*_{CNT}\left(\frac{2z}{h}+1\right) \qquad \text{with } -h/2 \le z \le h/2, \tag{9}$$

$$+ \text{For stiffeners } V_{CNT} = V^*_{CNT}\left(\frac{-2z+h}{h_l}+2\right) \text{ with } \quad h/2 \le z \le h/2+h_l. \tag{10}$$

In this paper, CNTs are designed in the x-direction of the plate. While the CNTs are always designed in the same direction as stiffeners

The effective elastic constants including elastic moduli and Poison's ratio can be estimated using the extended rule of the mixture

$$\begin{aligned} &E_{11} = \eta_1 V_{CNT} E^{CNT}_{11} + V_m E^m, \\ &\frac{\eta_2}{E_{22}} = \frac{V_{CNT}}{E^{CNT}_{22}} + \frac{V_m}{E^m}, \quad \frac{\eta_3}{G_{12}} = \frac{V_{CNT}}{G^{CNT}_{12}} + \frac{V_m}{G^m}, \quad \nu_{12} = V^*_{CNT}\nu^{CNT}_{12} + V_m\nu^m, \end{aligned} \tag{11}$$

where the superscripts CNT and m denote CNT and matrix, respectively. The performance parameters of CNTs denoted as η_1, η_2 and η_3, can be taken according to Shen et al. [1,4,6].

The oblique FG-CNTRC stiffeners are modeled by developing the smeared stiffener technique for the shear deformable laminated stiffeners. By employing this improved

technique, the internal forces of the FG-CNTRC plate stiffened by oblique FG-CNTRC stiffeners can be expressed as

$$\begin{Bmatrix} N_x \\ N_y \\ N_{xy} \\ M_x \\ M_y \\ M_{xy} \\ T_x \\ T_y \\ T_{xy} \end{Bmatrix} = \begin{bmatrix} A_{11} & A_{12} & 0 & B_{11} & B_{12} & 0 & C_{11} & C_{12} & 0 \\ A_{12} & A_{22} & 0 & B_{12} & B_{22} & 0 & C_{12} & C_{22} & 0 \\ 0 & 0 & A_{66} & 0 & 0 & B_{66} & 0 & 0 & C_{66} \\ B_{11} & B_{12} & 0 & D_{11} & D_{12} & 0 & E_{11} & E_{12} & 0 \\ B_{12} & B_{22} & 0 & D_{12} & D_{22} & 0 & E_{12} & E_{22} & 0 \\ 0 & 0 & B_{66} & 0 & 0 & D_{66} & 0 & 0 & E_{66} \\ C_{11} & C_{12} & 0 & E_{11} & E_{12} & 0 & L_{11} & L_{12} & 0 \\ C_{12} & C_{22} & 0 & E_{12} & E_{22} & 0 & L_{12} & L_{22} & 0 \\ 0 & 0 & C_{66} & 0 & 0 & E_{66} & 0 & 0 & L_{66} \end{bmatrix} \begin{Bmatrix} \varepsilon_x^0 \\ \varepsilon_y^0 \\ \gamma_{xy}^0 \\ \phi_{x,x} \\ \phi_{y,y} \\ \phi_{x,y} + \phi_{y,x} \\ -\lambda\left(\phi_{x,x} + w_{,xx}\right) \\ -\lambda\left(\phi_{y,y} + w_{,yy}\right) \\ -\lambda\left(\phi_{x,y} + \phi_{y,x} + 2w_{,xy}\right) \end{Bmatrix}, \quad (12)$$

where

$$\left(A_{ij}, B_{ij}, D_{ij}, C_{ij}, E_{ij}, L_{ij}\right) = \left(A_{ij}^P, B_{ij}^P, D_{ij}^P, C_{ij}^P, E_{ij}^P, L_{ij}^P\right) + \left(A_{ij}^S, B_{ij}^S, D_{ij}^S, C_{ij}^S, E_{ij}^S, L_{ij}^S\right), \quad (13)$$

and

$$\left(A_{ij}^P, B_{ij}^P, D_{ij}^P, C_{ij}^P, E_{ij}^P, L_{ij}^P\right) = \int_{-\frac{h}{2}}^{\frac{h}{2}} Q_{ij}^P(1,\ z,\ z^2,\ z^3, z^4, z^6)\mathrm{d}z, \quad (14)$$

and the stiffnesses of stiffeners can be calculated by

$$\begin{bmatrix} \overline{A}_{11} & \overline{B}_{11} & \overline{C}_{11} \\ \overline{B}_{11} & \overline{D}_{11} & \overline{E}_{11} \\ \overline{C}_{11} & \overline{E}_{11} & \overline{L}_{11} \end{bmatrix} = \begin{bmatrix} A_{11}^{St} & B_{11}^{St} & C_{11}^{St} \\ B_{11}^{St} & D_{11}^{St} & E_{11}^{St} \\ C_{11}^{St} & E_{11}^{St} & L_{11}^{St} \end{bmatrix} - \begin{bmatrix} A_{12}^{St} & 0 & B_{12}^{St} & 0 & C_{12}^{St} & 0 \\ B_{12}^{St} & 0 & D_{12}^{St} & 0 & E_{12}^{St} & 0 \\ C_{12}^{St} & 0 & E_{12}^{St} & 0 & L_{12}^{St} & 0 \end{bmatrix} \begin{bmatrix} A_{22}^{St} & 0 & B_{22}^{St} & 0 & C_{22}^{St} & 0 \\ 0 & A_{66}^{St} & B_{26}^{St} & B_{66}^{St} & 0 & C_{66}^{St} \\ B_{22}^{St} & 0 & D_{22}^{St} & 0 & E_{22}^{St} & 0 \\ 0 & B_{66}^{St} & 0 & D_{66}^{St} & 0 & E_{66}^{St} \\ C_{22}^{St} & 0 & E_{22}^{St} & 0 & C_{66}^{St} & 0 \\ 0 & L_{22}^{St} & 0 & E_{66}^{St} & 0 & L_{66}^{St} \end{bmatrix}^{-1} \begin{bmatrix} A_{12}^{St} & B_{12}^{St} & C_{12}^{St} \\ 0 & 0 & 0 \\ B_{12}^{St} & D_{12}^{St} & E_{12}^{St} \\ 0 & 0 & 0 \\ C_{12}^{St} & E_{12}^{St} & L_{12}^{St} \\ 0 & 0 & 0 \end{bmatrix}, \quad (15)$$

where $\left(A_{ij}^{St}, B_{ij}^{St}, D_{ij}^{St}, C_{ij}^{St}, E_{ij}^{St}, L_{ij}^{St}\right) = \dfrac{b_l}{d_l} \displaystyle\int_{\Omega} Q_{ij}^{St} \left(1, z, z^2, z^3, z^4, z^6\right) \mathrm{d}z, (i, j = 1, 2, 6).$

The expressions of the shear forces are also obtained as

$$\begin{aligned} Q_x &= H_{44} w_{,x} + H_{44}\phi_x, \quad Q_y = H_{55} w_{,y} + H_{55}\phi_y, \\ S_x &= H_{66} w_{,x} + H_{66}\phi_x, \quad S_y = H_{77} w_{,y} + H_{77}\phi_y, \end{aligned} \quad (16)$$

where

$$(H_{44}, H_{55}, H_{66}, H_{77}) = \left(H_{44}^P, H_{55}^P, H_{66}^P, H_{77}^P\right) + \left(H_{44}^S, H_{55}^S, H_{66}^S, H_{77}^S\right), \tag{17}$$

$$H_{44}^P = \int_{-\frac{h}{2}}^{\frac{h}{2}} Q_{44}^P \mathrm{d}z - 3\lambda \int_{-\frac{h}{2}}^{\frac{h}{2}} Q_{44}^P z^2 \mathrm{d}z, \;\; H_{55}^P = \int_{-\frac{h}{2}}^{\frac{h}{2}} Q_{55}^P \mathrm{d}z - 3\lambda \int_{-\frac{h}{2}}^{\frac{h}{2}} Q_{55}^P z^2 \mathrm{d}z, \tag{18}$$

$$H_{66}^P = \int_{-\frac{h}{2}}^{\frac{h}{2}} Q_{44}^P z^2 \mathrm{d}z - 3\lambda \int_{-\frac{h}{2}}^{\frac{h}{2}} Q_{44}^P z^4 \mathrm{d}z, \;\; H_{77}^P = \int_{-\frac{h}{2}}^{\frac{h}{2}} Q_{55}^P z^2 \mathrm{d}z - 3\lambda \int_{-\frac{h}{2}}^{\frac{h}{2}} Q_{55}^P z^4 \mathrm{d}z, \tag{19}$$

for the case of x-direction FG-CNTRC plate with x-direction stiffeners:

$$\bar{H}_{44} = \frac{b_l}{d_l}\left(\int_\Omega Q_{44}^S \mathrm{d}z - 3\lambda \int_\Omega Q_{44}^S z^2 \mathrm{d}z\right), \bar{H}_{66} = \frac{b_l}{d_l}\left(\int_\Omega Q_{44}^S z^2 \mathrm{d}z - 3\lambda \int_\Omega Q_{44}^S z^4 \mathrm{d}z\right), \tag{20}$$
$$\bar{H}_{55} = 0, \quad \bar{H}_{77} = 0,$$

and, for the case of y-direction FG-CNTRC plate with y-direction stiffeners

$$\bar{H}_{55} = \frac{b_l}{d_l}\left(\int_\Omega Q_{44}^S \mathrm{d}z - 3\lambda \int_\Omega Q_{44}^S z^2 \mathrm{d}z\right), \bar{H}_{77} = \frac{b_l}{d_l}\left(\int_\Omega Q_{44}^S z^2 \mathrm{d}z - 3\lambda \int_\Omega Q_{44}^S z^4 \mathrm{d}z\right), \tag{21}$$
$$\bar{H}_{44} = 0, \quad \bar{H}_{66} = 0,$$

with Ω is the interval of integration of stiffeners.

$$A_{11}^S = 2\bar{A}_{11}\cos^4\theta, \;\; A_{12}^S = 2\bar{A}_{11}\sin^2\theta\cos^2\theta, \; A_{22}^S = 2\bar{A}_{11}\sin^4\theta, \;\; A_{66}^S = 2\bar{A}_{11}\sin^2\theta\cos^2\theta,$$
$$B_{11}^S = 2\bar{B}_{11}\cos^4\theta, \;\; B_{12}^S = 2\bar{B}_{11}\sin^2\theta\cos^2\theta, B_{22}^S = 2\bar{B}_{11}\sin^4\theta, \;\; B_{66}^S = 2\bar{B}_{11}\sin^2\theta\cos^2\theta,$$
$$C_{11}^S = 2\bar{C}_{11}\cos^4\theta, \;\; C_{12}^S = 2\bar{C}_{11}\sin^2\theta\cos^2\theta, \; C_{22}^S = 2\bar{C}_{11}\sin^4\theta, \;\; C_{66}^S = 2\bar{C}_{11}\sin^2\theta\cos^2\theta,$$
$$D_{11}^S = 2\bar{D}_{11}\cos^4\theta, \;\; D_{12}^S = 2\bar{D}_{11}\sin^2\theta\cos^2\theta, D_{22}^S = 2\bar{D}_{11}\sin^4\theta, \;\; D_{66}^S = 2\bar{D}_{11}\sin^2\theta\cos^2\theta,$$
$$E_{11}^S = 2\bar{E}_{11}\cos^4\theta, \;\; E_{12}^S = 2\bar{E}_{11}\sin^2\theta\cos^2\theta, \; E_{22}^S = 2\bar{E}_{11}\sin^4\theta, \;\; E_{66}^S = 2\bar{E}_{11}\sin^2\theta\cos^2\theta,$$
$$L_{11}^S = 2\bar{L}_{11}\cos^4\theta, \;\; L_{12}^S = 2\bar{L}_{11}\sin^2\theta\cos^2\theta, \; L_{22}^S = 2\bar{L}_{11}\sin^4\theta, \;\; L_{66}^S = 2\bar{L}_{11}\sin^2\theta\cos^2\theta,$$
$$H_{44}^S = 2\bar{H}_{44}\sin^2\theta, \;\; H_{55}^S = 2\cos^2\theta\bar{H}_{55}, \;\; H_{66}^S = 2\bar{H}_{66}\sin^2\theta, \;\; H_{77}^S = 2\cos^2\theta\bar{H}_{77},$$

The system of equilibrium equations of obliquely stiffened FG-CNTRC plate respecting Reddy's HSDPT [11] can be applied by

$$\begin{aligned}
&N_{x,x} + N_{xy,y} = 0,\\
&N_{xy,x} + N_{y,y} = 0,\\
&Q_{x,x} + Q_{y,y} - 3\lambda\left(S_{x,x} + S_{y,y}\right) + \lambda\left(T_{x,xx} + 2T_{xy,xy} + T_{y,yy}\right) + N_x\left(w_{,xx} + \bar{w}_{,xx}\right)\\
&\qquad + 2N_{xy}\left(w_{,xy} + \bar{w}_{,xy}\right) + N_y\left(w_{,yy} + \bar{w}_{,yy}\right) = 0,\\
&M_{x,x} + M_{xy,y} - Q_x + 3\lambda S_x - \lambda\left(T_{x,x} + T_{xy,y}\right) = 0,\\
&M_{xy,x} + M_{y,y} - Q_y + 3\lambda S_y - \lambda\left(T_{xy,x} + T_{y,y}\right) = 0,
\end{aligned} \tag{22}$$

To satisfy the two first equations of Eq. (22) the stress function $f(x,y)$ is introduced as

$$N_x = f_{,yy}, \quad N_y = f_{,xx}, \quad N_{xy} = -f_{,xy}. \tag{23}$$

The compatibility equation is presented in the form

$$\begin{aligned} &A_{11}^* f_{,xxxx} + a_1 f_{,xxyy} + A_{22}^* f_{,yyyy} - \left(w_{,xy}\right)^2 + w_{,xx} w_{,yy} \\ &\quad - C_{21}^* \lambda w_{,xxxx} + w_{,xx} \bar{w}_{,yy} - 2 w_{,xy} \bar{w}_{,xy} + w_{,yy} \bar{w}_{,xx} + a_2 w_{,xxyy} \\ &\quad - C_{12}^* \lambda w_{,yyyy} + a_3 \phi_{x,xxx} + a_4 \phi_{x,xyy} + a_5 \phi_{y,xxy} + a_6 \phi_{y,yyy} = 0. \end{aligned} \tag{24}$$

The equilibrium equation system (22) can be rewritten by

$$\begin{aligned} &-\lambda C_{21}^* f_{,xxxx} + b_1 f_{,xxyy} - \lambda C_{12}^* f_{,yyyy} - \lambda^2 L_{11}^* w_{,xxxx} + b_2 w_{,xxyy} + b_3 \phi_{x,xxx} + b_4 \phi_{x,xyy} \\ &\quad + b_5 \phi_{y,xxy} + b_6 \phi_{y,yyy} - \lambda^2 L_{22}^* w_{,yyyy} + \left(w_{,yy} + \bar{w}_{,yy}\right) f_{,xx} - 2\left(w_{,xy} + \bar{w}_{,xy}\right) f_{,xy} \\ &\quad + \left(w_{,xx} + \bar{w}_{,xx}\right) f_{,yy} + b_7 w_{,xx} + b_8 w_{,yy} + b_7 \phi_{x,x} + b_8 \phi_{y,y} = 0, \end{aligned} \tag{25}$$

$$\begin{aligned} &c_1 f_{,xxx} + c_2 f_{,xyy} + c_3 w_{,xxx} + c_4 w_{,xyy} + c_5 \phi_{x,xx} \\ &\quad + c_6 \phi_{x,yy} + c_7 \phi_{y,xy} + c_8 w_{,x} + 3\lambda H_{66} \phi_x - H_{44} \phi_x = 0, \end{aligned} \tag{26}$$

$$\begin{aligned} &d_1 f_{,xxy} + d_2 f_{,yyy} + d_3 w_{,xxy} + d_4 w_{,yyy} + d_5 \phi_{x,xy} \\ &\quad + d_6 \phi_{y,xx} + d_7 \phi_{y,yy} + d_8 w_{,y} + 3\lambda H_{77} \phi_y - H_{55} \phi_y = 0, \end{aligned} \tag{27}$$

In this paper, the stiffened plate is considered with four simply supported and freely movable edges, and the approximation solutions of deflection, rotations and imperfection are used in the form

$$\begin{aligned} w &= W \sin \alpha x \sin \beta y, \qquad \bar{w} = \xi h \sin \alpha x \sin \beta y, \\ \phi_x &= \Phi_x \cos \alpha x \sin \beta y, \quad \phi_y = \Phi_y \sin \alpha x \cos \beta y, \end{aligned} \tag{28}$$

with ξ is the dimensionless imperfection, $\alpha = m\pi/a, \beta = n\pi/b$; m and n are numbers of half waves in x and y directions, respectively.

By substituting Eq. (28) into Eq. (24), the expression of stress function is expressed as

$$f = f_1 \cos 2\alpha x + f_2 \cos 2\beta y + f_3 \sin \alpha x \sin \beta y + \frac{1}{2} N_{x0} y^2 + \frac{1}{2} N_{y0} x^2. \tag{29}$$

Substituting Eqs. (28) and (29) into Eqs. (25)–(27), the algebraic equilibrium equations can be obtained using the Galerkin procedure, as

$$\begin{aligned} &y_2 q + \left(y_1 N_{x0} + y_3 N_{y0}\right)(h\xi + W) + y_6 \Phi_y + y_5 \Phi_x + y_4 \left(X_1 \Phi_x + X_2 \Phi_y\right)(h\xi + W) \\ &\quad + y_7 (2h\xi + W) W (h\xi + W) + y_8 (2h\xi + W) W + y_4 X_3 W (h\xi + W) + y_9 W + y_{10} W^3 = 0, \\ &z_1 \Phi_x + z_2 \Phi_y + z_3 (2h\xi + W) W + z_4 W = 0, \\ &z_5 \Phi_x + z_6 \Phi_y + z_7 (2h\xi + W) W + z_8 W = 0. \end{aligned} \tag{30}$$

The axial compression load P_x from Eq. (30) is determined

$$P_x = \frac{1}{\left(\xi + \frac{W}{h}\right)(hy_1)} \left[\begin{array}{l} y_{10}\left(\frac{W}{h}\right)^3 h^2 + \left(2\xi + \frac{W}{h}\right)\frac{W}{h}\left(\xi + \frac{W}{h}\right)e_5 \\ +e_6\left(2\xi + \frac{W}{h}\right)\frac{W}{h} + e_8\frac{W}{h}\left(\xi + \frac{W}{h}\right) + e_7\frac{W}{h} \end{array} \right]. \tag{31}$$

When $\bar{W} \to 0$ and $\xi = 0$, the upper axial compression load can be written as

$$P_x^{upper} = e_7/(hy_1). \tag{32}$$

3. NUMERICAL RESULTS AND DISCUSSIONS

In this part, the dimensionless critical axial compressive buckling loads $\bar{P}_x^{cr} = P_x^{cr}b^2 / E_0^m h^2$ of FG-CNTRC plates of the current method are validated using the ones of Zhang et al. [2] and Zghal et al. [3] (see Table 1). As can be perceived, the perfect agreements are obtained, and the present results coincide with the previous results.

Table 1. Validation of dimensionless critical compressive buckling loads $\bar{P}_x^{cr} = P_x^{cr}b^2 \Big/ E_0^m h^2$ of FG-CNTRC plates $(a/b = 1, a/h = 100, (m,n) = (1,1))$

		Zhang et al. [2]	Zghal et al. [3]	Present
UD	0.11	37.86	39.45	39.83
	0.14	49.14	49.52	49.78
	0.17	57.54	60.62	61.22
FG-X	0.11	56.71	57.23	57.67
	0.14	71.77	72.17	72.77
	0.17	83.74	88.28	88.65
FG-O	0.11	21.32	21.50	21.61
	0.14	26.40	26.60	26.82
	0.17	31.22	32.76	32.95

In this paper, the material properties of FG-CNTRC with the matrix made by Poly methyl methacrylate (PMMA) and the reinforcement material is single-walled CNTs are applied according to the research of Shen et al. [1,4,6]. The environment temperature is considered at room temperature ($T = 300$ K) in all investigations.

Table 2 presents the effects of CNT distribution laws on the critical buckling loads of FG-CNTRC plates. As can be seen that the largest critical buckling loads can be obtained for the FG-V distribution type, and the smallest is obtained for the FG-Λ distribution type. This is suitable for the CNT distribution presented in Fig. 1. For the FG-V distribution type the large quantity of CNT is distributed near the two outer surfaces of the plate

and stiffeners. Oppositely, they are concentrated mainly in the position between the shell and stiffeners for FG-Λ distribution type.

Table 2. Effects of CNT distribution laws and stiffener angle on the critical buckling loads (GPa) of FG-CNTRC plates ($V^*_{CNT} = 0.17$, $a = b = 20h$, $\xi = 0$, $m = n = 1$, $h = 0.002$ m, $h_l = 0.003$ m, $b_l = 0.002$ m, $d_l = 0.004$ m)

θ (°)	UD	FG-X	FG-V	FG-Λ	FG-O
10	2.478	2.420	3.212	1.646	2.422
13	2.578	2.512	3.342	1.766	2.565
14	2.577	2.057	3.306	1.790	2.577
16	2.532	2.453	3.134	1.812	2.552
20	2.305	2.207	2.559	1.761	2.340
30	1.578	1.492	1.411	1.345	1.555

Table 2 and Fig. 2 also investigated the stiffener angle on the critical buckling loads of FG-CNTRC plates. When the stiffener angle increases, the critical buckling loads of plates increase, then decreases after achieving the maximal values. The optimal obtained angles are different for different distribution laws of CNT. Subsequent figures are shown with the optimal stiffener angles.

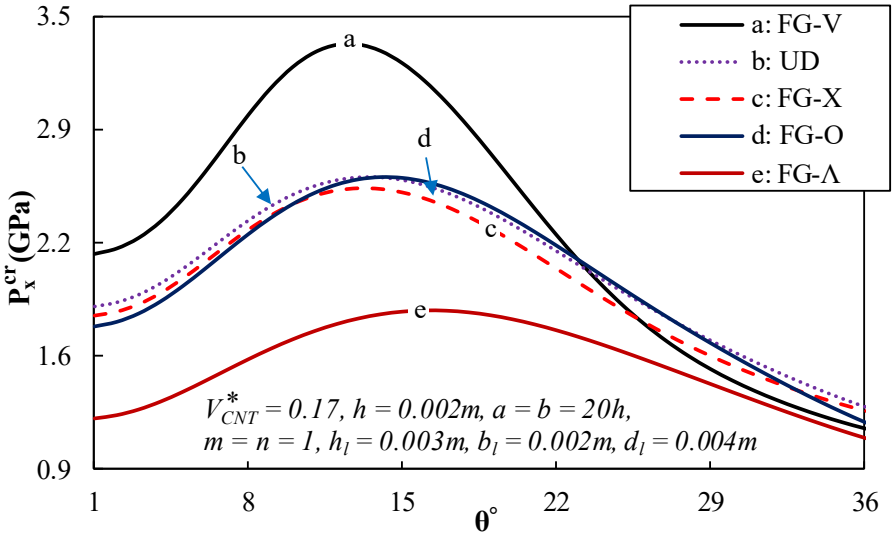

Fig. 2. Effects of stiffener angle on the critical buckling loads of FG-CNTRC plates

Effects of stiffener and imperfection on the postbuckling curves of FG-CNTRC plates are investigated in Fig. 3. The results show that the postbuckling strength of obliquely

stiffened plates is much larger than that of unstiffened plates for both perfect and imperfect cases. A slight snap-through can be observed for stiffened plates, while it can not be obtained for unstiffened plates.

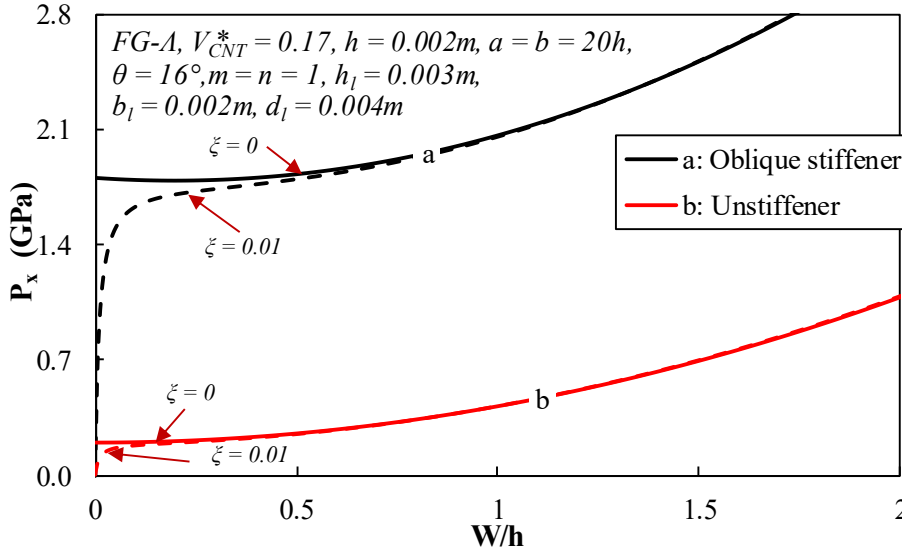

Fig. 3. Effects of stiffener and imperfection on the postbuckling curves of FG-CNTRC plates

Fig. 4 presents the effects of CNT distribution laws on the postbuckling curves of stiffened FG-CNTRC plates. The snap-through phenomenon can be clearly observed in almost distribution law cases. The critical buckling load of the FG-V distribution law case is the largest, however the largest snap-through can be also obtained for this case. Effects of CNT volume fraction on the postbuckling curves of stiffened FG-CNTRC plates are investigated in Fig. 5. The postbuckling strength of plates considerably increases when the CNT volume fraction increases. Fig. 6 presents the effects of a/h ratio on the postbuckling curves of obliquely stiffened FG-CNTRC plates. As can be seen that when the a/h ratio increases, i.e. the relative thickness of the plate increases, the postbuckling strength increases clearly, however, the snap-through also considerably increases for thicker plates.

Effects of stiffener width and stiffener distance on the postbuckling curves of FG-CNTRC plates are investigated in Figs. 7 and 8. Of course, as stiffener width increases or stiffener distance decreases, postbuckling strength increases dramatically. The postbuckling curves tend to move away from each other as the deflection increases.

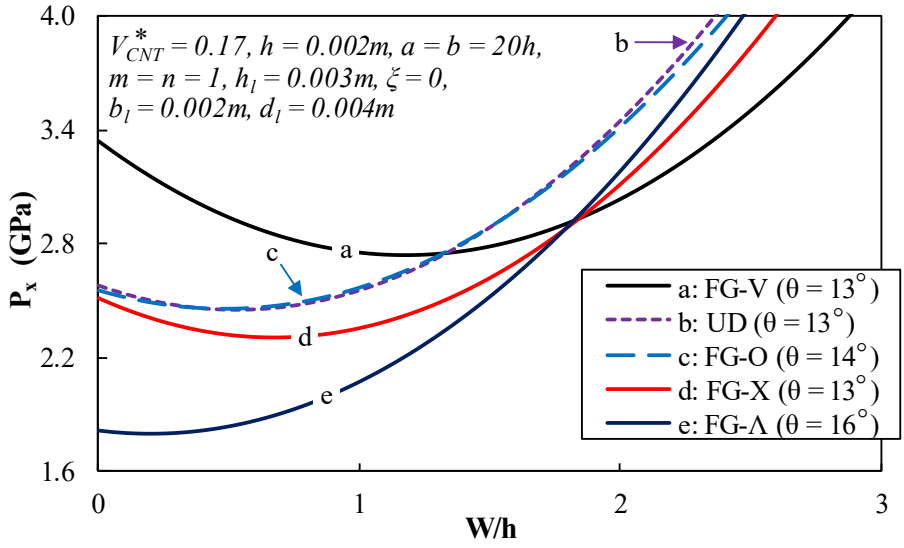

Fig. 4. Effects of CNT distribution laws on the postbuckling curves of FG-CNTRC plates

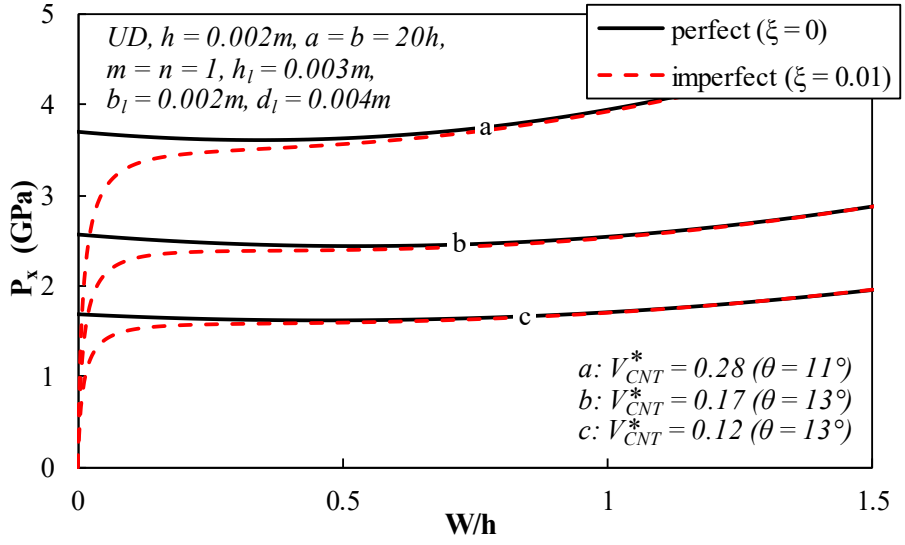

Fig. 5. Effects of CNT volume fraction on the postbuckling curves of FG-CNTRC plates

Fig. 9 investigated the effects of stiffener height on the postbuckling curves of stiffened FG-CNTRC imperfect plates. In the small deflection region, the postbuckling strength is larger with the larger height of the stiffeners. Oppositely, the snap-through also increases when the stiffener height increases. This leads to the reverse order of postbuckling strength can be observed in the large region of deflection.

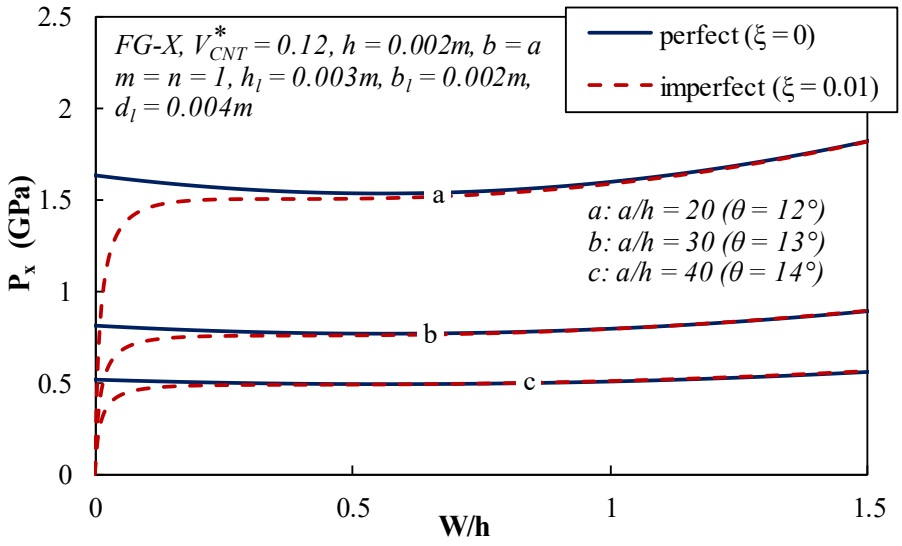

Fig. 6. Effects of a/h ratio on the postbuckling curves of FG-CNTRC plates

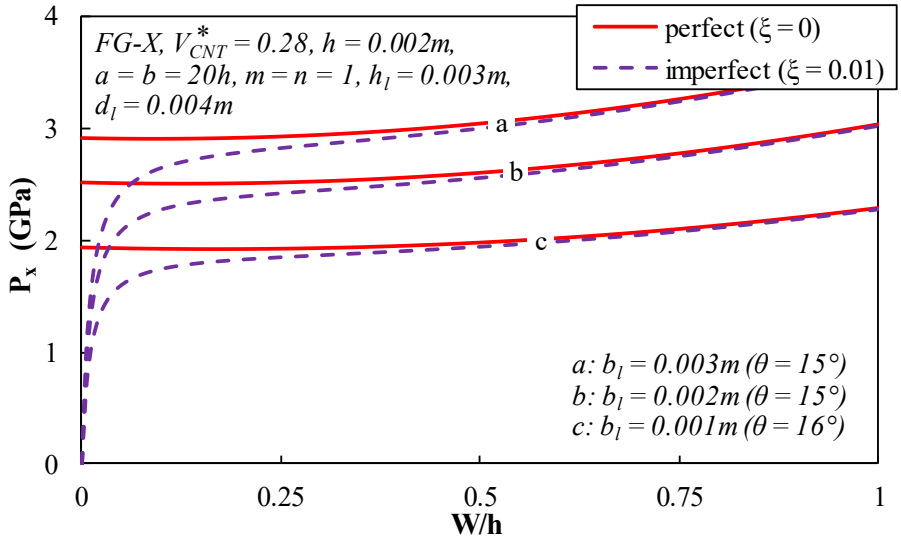

Fig. 7. Effects of stiffener width on the postbuckling curves of FG-CNTRC plates

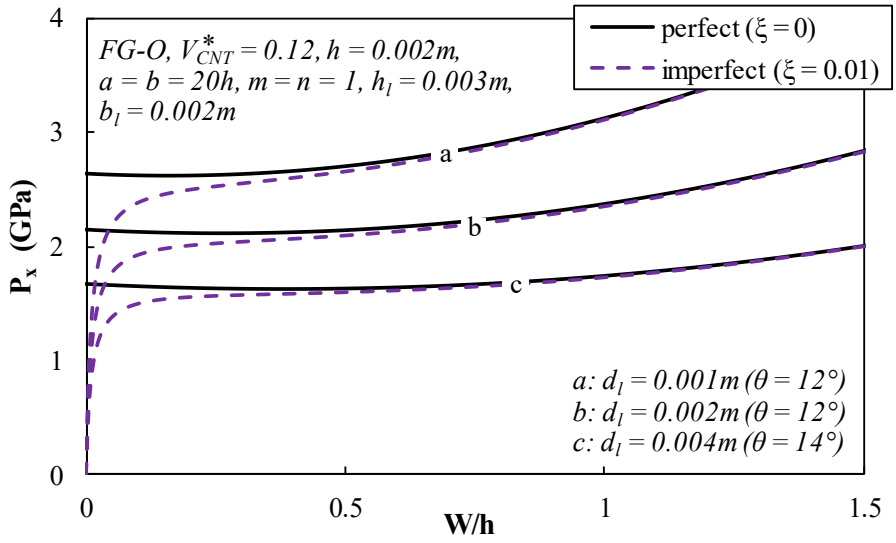

Fig. 8. Effects of stiffener distance on the postbuckling curves of FG-CNTRC plates

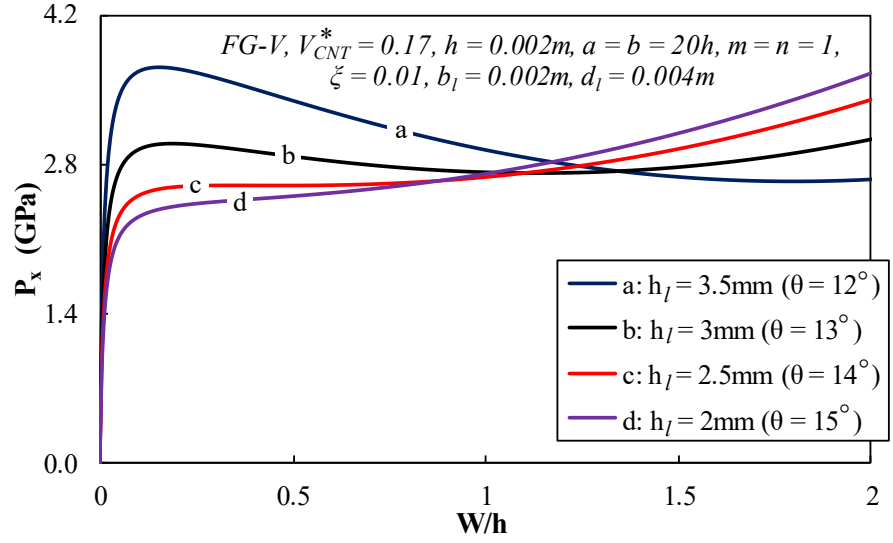

Fig. 9. Effects of stiffener height on the postbuckling curves of FG-CNTRC plates

4. CONCLUSIONS

The nonlinear buckling behavior of FG-CNTRC plates stiffened by oblique FG-CNTRC stiffeners under axial compression load has been presented and investigated. In general, the obtained buckling behavior of the plates is complex with some notable points as follows:

(i) The critical buckling load and postbuckling strength of the plates considerably increase with the FG-CNTRC stiffeners;

(ii) With the present stiffener design, for stiffened plates, the effects of the stiffeners on the critical loads of the FG-V plates are the largest;

(iii) Snap-through can be clearly observed for obliquely stiffened plates, oppositely, this can be obtained for unstiffened plates;

(iv) The geometrical and material parameters significantly influence the nonlinear postbuckling curve of plates and the tendency of the postbuckling curves of the plates under axial compressive load are much different.

DECLARATION OF COMPETING INTEREST

The authors declare that they have no known competing financial interests or personal relationships that could have appeared to influence the work reported in this paper.

FUNDING

This research received no specific grant from any funding agency in the public, commercial, or not-for-profit sectors.

REFERENCES

[1] H.-S. Shen and Z. H. Zhu. Buckling and postbuckling behavior of functionally graded nanotube-reinforced composite plates in thermal environments. *Computers, Materials & Continua (CMC)*, **18**, (2), (2010), pp. 155–182.

[2] L. W. Zhang, Z. X. Lei, and K. M. Liew. Buckling analysis of FG-CNT reinforced composite thick skew plates using an element-free approach. *Composites Part B: Engineering*, **75**, (2015), pp. 36–46. https://doi.org/10.1016/j.compositesb.2015.01.033.

[3] S. Zghal, A. Frikha, and F. Dammak. Mechanical buckling analysis of functionally graded power-based and carbon nanotubes-reinforced composite plates and curved panels. *Composites Part B: Engineering*, **150**, (2018), pp. 165–183. https://doi.org/10.1016/j.compositesb.2018.05.037.

[4] H.-S. Shen and C.-L. Zhang. Thermal buckling and postbuckling behavior of functionally graded carbon nanotube-reinforced composite plates. *Materials & Design*, **31**, (2010), pp. 3403–3411. https://doi.org/10.1016/j.matdes.2010.01.048.

[5] M. Mirzaei and Y. Kiani. Thermal buckling of temperature dependent FG-CNT reinforced composite plates. *Meccanica*, **51**, (2015), pp. 2185–2201. https://doi.org/10.1007/s11012-015-0348-0.

[6] H.-S. Shen and H. Wang. Nonlinear vibration of compressed and thermally postbuckled nanotube-reinforced composite plates resting on elastic foundations. *Aerospace Science and Technology*, **64**, (2017), pp. 63–74. https://doi.org/10.1016/j.ast.2017.01.017.

[7] M. Mirzaei and Y. Kiani. Nonlinear free vibration of FG-CNT reinforced composite plates. *Structural Engineering and Mechanics*, **64**, (3), (2017), pp. 381–390.

[8] V. H. Nam, D. T. Dong, N. T. Phuong, and H. D. Tuan. Nonlinear thermo-mechanical stability of multilayer-FG plates reinforced by orthogonal and oblique stiffeners according to FSDT. *Journal of Reinforced Plastics and Composites*, **38**, (2019), pp. 521–536. https://doi.org/10.1177/0731684419831650.

[9] V. H. Nam, N. T. Phuong, D. T. Dong, N. T. Trung, and N. V. Tue. Nonlinear thermo-mechanical buckling of higher-order shear deformable porous functionally graded material plates reinforced by orthogonal and/or oblique stiffeners. *Proceedings of the Institution of Mechanical Engineers, Part C: Journal of Mechanical Engineering Science*, **233**, (2019), pp. 6177–6196. https://doi.org/10.1177/0954406219861658.

[10] D. T. Dong, V. H. Nam, N. T. Trung, N. T. Phuong, and V. T. Hung. Nonlinear thermo-mechanical buckling of sandwich FGM oblique stiffened plates with nonlinear effect of elastic foundation. *Journal of Thermoplastic Composite Materials*, **35**, (2020), pp. 1441–1467. https://doi.org/10.1177/0892705720935957.

[11] C. M. Wang, J. N. Reddy, and K. H. Lee. Introduction. In *Shear Deformable Beams and Plates*, pp. 1–7. Elsevier, (2000). https://doi.org/10.1016/b978-008043784-2/50001-0.